RSC Advances

ROYAL SOCIETY OF CHEMISTRY

www.rsc.org/advances

A mechanistic approach for superoxide radicals and singlet oxygen mediated enhanced photocatalytic dye degradation by selenium doped ZnS nanoparticles

Soumita Talukdar, Raj Kumar Dutta*

Department of Chemistry, Indian Institute of Technology Roorkee, Roorkee 247667, India

* Corresponding Author, Email address: duttafcy@iitr.ac.in (R.K. Dutta), Tel: +91 1332 285280, Fax: +91 1332 286202

Abstract

Structural modification of semiconductor type nanoparticles by doping with metals and non-metals renders versatility of a material. Here we report synthesis of less than 4 nm sized nanocrystalline selenium doping in ZnS nanoparticles (Se doped ZnS NPs) by chemical precipitation method, and the mechanism involved in drastic improvement in its photocatalytic activity as compared to pristine ZnS nanoparticles. Array of characterization techniques, including X-ray diffraction (XRD), high resolution transmission electron microscopy (HRTEM), Diffused reflectance spectroscopy (DRS), Fourier transformed infrared spectroscopy (FT-IR), zeta potential and BET surface area measurement were used to confirm synthesis of stable Se doped ZnS NPs with large surface area. Selenium doping not only led to lattice distortion in the ZnS lattice but it also resulted in band gap narrowing due to incorporation of defects sites within the forbidden gap, supported by fluorescence emission spectroscopy studies. These modified properties in Se doped ZnS NPs were important for enhanced sunlight induced photocatalytic activity, demonstrated via degradation of trypan blue dye. Compared to the pristine ZnS nanoparticles, the kinetic study revealed a three folds increase in the efficiency of the dye

degradation and about seven folds increase in the rate of dye degradation. The mechanism of the dye degradation is studied in terms of scavenging of as generated reactive oxygen species (ROS) in the reaction medium. The *p*-benzoquinone assay and sodium azide assay confirmed that the dye degradation by Se doped ZnS was due to production of superoxide radicals and singlet oxygen species, respectively which were generated due to interaction of photoexcited conduction band electrons with molecular oxygen at the surface of the nanoparticles. The proposed mechanism is supported by the theoretical calculation of band structure of Se doped ZnS nanoparticles.

Keywords: Selenium, Zinc sulphide nanoparticles, Superoxide radicals, Singlet oxygen, Photocatalytic dye degradation.

1. Introduction

Wastewater effluents from textile industries are severe threat to environment and human health and hence demand suitable remediation technology.[1,2] In this regard, semiconductor type nanomaterials have rapidly evolved as an efficient heterogenous photocatalyst for wastewater treatment.[3-7] Semiconductor nanomaterials as photocatalyst for dye degradation is not only economically favorable and technologically sustainable, but it is also environmentally friendlier as compared to the conventional oxidation by bleaching or advanced oxidation process (AOP) based on Fenton's chemistry using UV light source and strong oxidizing agents like ozone or by electron beam irradiation.[8-10] The photoinduced reaction in a semiconductor nanoparticle is initiated by absorption of light energy greater than or equal to the band gap of the material to generate the valence band holes (h^+) and conduction band electrons (e^-), which could either re-

combine or transport to the surface of the nanoparticles.[11] Typically, the photocatalytic dye degradation by semiconductor type nanomaterials is an oxidation process where the free or trapped holes oxidize the water molecule directly to produce hydroxyl radicals or undergoes indirect oxidation by ROS (e.g., singlet oxygen, superoxide radicals), which are formed due to reduction of molecular oxygen by free or trapped electron.[12,13] Various experimental studies comprising electron spin resonance spectroscopy (ESR), laser induced fluorescence spectroscopy, fluorescent probes are reported for establishing the mechanism of ROS generation and subsequent dye degradation.[14-16] Most of these studies are based on the usages of various metal oxide nanoparticles, in presence and absence of co-catalysts like H_2O_2 or $S_2O_8^{2-}$.[17-19] The most important feature regarding dye degradation is to achieve faster rate of degradation rate especially for industrial dye which comprises of complex structure containing one or more azo (-N=N-) chromogenic groups which are stable against conventional methods of degradation.[20]

It may be remarked here that there exist enormous scope for exploring materials other than metal oxides as photocatalyst for waste water treatment, and particularly to explore dye degradation.[21,22] In this regard, ZnS nanoparticles are investigated as an efficient photocatalyst for degradation of organic pollutants in wastewater treatment.[23] However, the major disadvantage of using ZnS NPs as photocatalyst is attributed to its wide band gap (3.68 eV for bulk or higher for NPs). This would therefore require ultraviolet light irradiation and hence imposes a self limiting constraint for utilizing solar energy spectrum. However, conjugation of polymer-ZnS complex and doping of ZnS nanocrystals with Cu, Ni and Pb were reported to exhibit photocatalytic dye degradation using visible light.[24,25] The other challenge for ZnS NPs has been attributed to its route of synthesis, where chemical precipitation method is recommended to be followed by heat treatment under nitrogen atmosphere is required.[26]

Here we report the mechanism of photocatalytic dye degradation by Se doped ZnS nanoparticles. Selenium was chosen in this study for its favorable photoelectric conversion property.[27-29] In addition, it is non-toxic in nature and therefore suitable to environmental applications.[30] The mechanism of enhanced ability of photocatalytic degradation of trypan blue (a model azo dye) has been discussed in the light of structural changes in ZnS due to Se doping and ROS generation in aqueous medium when exposed to sunlight.

2. Materials and Method

2.1. Chemicals

Zinc acetate, sodium sulphide (Na_2S), mercaptoacetic acid (MAA) or thioglycolic acid ($HSCH_2COOH$), selenium dioxide (SeO_2), tryphan blue dye, terephthalic acid $(C_6H_4(COOH))_2$, ethanol (C_2H_5OH), sodium azide (NaN_3), *p*-benzoquinone, dimethyl sulphoxide (DMSO), hydrogen peroxide (H_2O_2) and concentrated hydrochloric acid (HCl) were procured from Himedia Chemicals Pvt. Ltd. India. All reagents and precursors used in this study were of analytical grade and were used without further purification. All aqueous solutions used in this study were prepared with de-ionized water (Millipore).

2.2. Synthesis of ZnS NPs and Se doped ZnS NPs

Two batches selenium doped ZnS NPs were prepared by chemical precipitation method, where 11 mg (X) and 22 mg (Y) of selenium dioxide were respectively mixed in 50 mL of 20 mM of zinc acetate solution and stirred for 1 h at 60-80 ^oC, maintained at pH 7. Similarly, 60 mM solution of Na_2S as a precipitating agent was prepared in deionized water. To this solution, 175 µL of 40 mM mercaptoacetic acid (MAA) was added as a capping agent. This mixture was

homogenized by magnetic stirring and was added drop wise to the solution containing zinc acetate and selenium dioxide under stirring condition. First a brownish turbid solution formed to which 0.5 M solution of NaOH was added. This mixture was subjected to stirring till a light yellow precipitate of ZnS nanoparticles doped with Se was formed (Se doped ZnS NPs). It may be suggested here that mercaptoacetic acid played the role of capping agent by forming S-S bond with ZnS. The nanoparticles were recovered by centrifugation and washed with ethanol several times to remove impurities and then air dried overnight. Similarly, pristine ZnS nanoparticles (ZnS NPs) were synthesized without adding selenium dioxide in the above protocol. The actual concentration of selenium and zinc in the batches of Se doped ZnS NPs were analyzed by atomic absorption spectrometry (Perkin Elmer Aanalyst 800) after digesting Se doped ZnS NPs with a mixture of concentrated nitric acid and hydrochloric acid (1:3 molar ratio). Accurately weighed 50 mg of Se doped ZnS NPs was treated with 15 mL of the acid mixture and heated till brown fumes ceased to evolve. The digest was slowly cooled to room temperature and the volume was made up to 1000 mL by serial dilution in volumetric flask. Three sets of digestion of respective X and Y batches of Se doped ZnS NPs were performed for independent triplicate analysis. The concentrations of selenium in respective batches of the digested samples were determined in triplicate against the calibration plot obtained by analysing known concentrations of standard selenium (Merck). The concentration of Se in Se doped ZnS NPs was calculated using the formula given below:

Se (wt %) = [mass of Se in acid digest (mg)/ mass of Se doped ZnS NPs digested (mg)] x 100

where, mass of Se in acid digest = Se concentration measured by AAS (say, α mg/L) x volume correction (i.e., 1000 mL)

2.3. Characterization techniques

The X-ray diffraction measurements of the Se doped ZnS NPs and pristine ZnS NPs were recorded with Bruker ARS D8 Advance diffractometer. The instrument was operated at 40 kV where graphite monochromatized Cu-K_α X-rays (λ = 1.54 Å) was scanned at 2^o/min in a wide angle region from 10^o to 80^o on a 2θ scale. The morphology and particle size distribution of the nanoparticles were studied by high resolution transmission electron microscopy (HRTEM) coupled with element analysis facility by energy dispersive X-ray (EDX) analysis. The TEM studies were carried out using FEI Technai-G^2 microscope operated at an acceleration voltage of 200 kV. The samples for TEM were prepared by drop casting the nanoparticles dispersed in ethanol on to onto a 150 mesh copper grid. The Brunauer–Emmett–Teller (BET) specific surface area of the nanoparticles were measured by Quantachrome Nova 2200 analyzer at liquid nitrogen temperature using nitrogen adsorption–desorption method.

The optical band gap of the as-synthesized Se doped ZnS NPs and pristine ZnS NPs were determined from their respective UV-visible absorption spectra (Shimadzu UV1800). The emission spectra of the nanoparticles were recorded by Spectro-fluorimeter FLS 980 (HORIBA), in the wavelength range of 400-1500 nm, where the excitation wavelength was 680 nm. The Fourier transformed infrared (FT-IR) spectra were recorded on Thermo NICOLET 6700 FTIR in KBr pellets. The Zeta potential of the nanoparticles was recorded in aqueous medium by Malvern Zetasizer Nano ZS90.

2.4. Photocatalytic degradation study

Trypan blue dye solution (15 mg/L) was chosen as a test dye for sunlight induced photocatalytic degradation study by the batches of as-synthesized pristine ZnS NPs and Se doped ZnS NPs as

photocatalyst. All photocatalytic degradation experiments were carried out at IIT Roorkee (29°51′N; 77°53′E) in the month of April and May 2015. First, a batch of 0.8 mg/mL photocatalyst treated with 50 mL of the dye solution in dark. 1 mL of the aliquot was collected after specific time interval and the concentration of dye as measured by UV-visible spectrophotometer (Shimadzu UV-1800). A 15 % decrease in dye concentration was recorded and the adsorption-desorption equilibrium was attained within 60 min.

For studying photocatalytic dye degradation, the batches of dye solution treated with respective photocatalysts were first kept in dark for 60 min and then the experimental assembly was exposed to sunlight for 3 h. A kinetic study of dye degradation was performed by measuring the concentration of the dye solution at specific time interval. The absorbance of decolourized solution was measured at λ_{max} = 590 nm after centrifuge at 15000 rpm at 25 ^{o}C for 5 min in Beckman Coulter^{TM} Allegra TM X-22R centrifuge. Simultaneously a control kinetic experiment was conducted where the dye solution of same concentration, without treating with nanoparticles (as photocatalyst), was exposed to sunlight.

2.5. Reactive oxygen species (ROS) assay

Interaction of semiconductor nanoparticles, including ZnS in aqueous medium tends to generate reactive oxygen species (ROS), e.g., hydroxyl radicals ($OH^{\cdot}$), superoxide radicals ($O_2^{\cdot -}$ and singlet oxygen ($^1O_2$). The tentative generation of ROS were studied by the following methods:

2.5.1. Terepthalic Acid assay

The generation of hydroxyl radicals due to interaction of pristine and Se doped ZnS NPs in aqueous medium under the exposure to sunlight was determined by terepthalic acid assay.[30] The

batches of as-prepared nanoparticles (0.8 mg/mL) were dispersed in 2 mM terephthalic acid solution prepared in NaOH solution and was sonicated for 10 min and then exposed to the sunlight for 40 min. The hydroxyl radicals, if generated in the medium would form a product with terephthalic acid which is fluorescent in nature. After centrifuging the reaction mixture, the fluorescence emission spectrum of the product was measured using an excitation wavelength at λ= 315 nm. A control batch of dye solution without treating with nanoparticles was simultaneously exposed to sunlight to confirm that the dye degradation was not due to photolysis. A second control experiment was also performed in dark condition in presence of the nanoparticles to assess the chance of adsorption of dye on the nanoparticles.

2.5.2. Superoxide radical, singlet oxygen and hydroxyl radical scavenging

The generation of superoxide radicals ($O_2^{\cdot -}$), singlet oxygen ($^1O_2$) and hydroxyl radicals ($OH^{\cdot}$) in the reaction medium were determined by treating with their respective quenchers. In this regard, *p*-benzoquinone was used as a superoxide radical specific quencher;[31] sodium azide as singlet oxygen specific quencher;[32] and dimethyl sulphoxide as hydroxyl radical quencher.[33] If the dye degradation is triggered due to generation any of these ROS then the photocatalytic dye degradation would be inhibited in presence of their respective quenchers.

To assess the role of singlet oxygen the batches of trypan blue dye solution (concentration of 15 mg/L) were mixed with 10 mM, 50 mM and 100 mM and 200 mM sodium azide, respectively. These batches were then treated with Se doped ZnS NPs (0.8 mg/mL), respectively. A control experiment was run without adding sodium azide. After equilibrating the reaction mixture in dark followed by exposure to sunlight, the kinetics of dye degradation inhibition was studied by monitoring the intensity of the UV-visible absorption spectrum of the dye. Similarly, the

generation of hydroxyl radicals, if any in the reaction medium was determined by treating with dimethyl sulphoxide (DMSO), as a quencher. The methodology for DMSO based hydroxyl radical scavenging was same as that described for sodium azide assay. However, the methodology for *p*-benzoquinone based scavenging of superoxide radicals was different due to poor solubility of *p*-benzoquinone in water. Firstly, the commercially procured *p*-benzoquinone was re-crystallized in ethanol. The freshly prepared yellow coloured crystals of *p*-benzoquinone was dissolved in ethanol (98 %), which was mixed with the trypan blue solution prepared in deionized water so that the ethanol: water ratio was 1:9. To this dye solution, 0.8mg/ml of Se doped ZnS NPs was added and equilibrated in dark for 60 min followed by exposure to sunlight for 3 h. A control experiment was performed where the dye solution in ethanol-water system without treating with Se doped ZnS NPs was monitored. Since ethanol evaporates faster than water so it was necessary to maintain the ethanol:water ratio in dye solution throughout the period of kinetic study by adding optimized volume of ethanol. The inhibition of dye degradation due to addition of *p*-benzoquinone was determined from a kinetic study as described above.

3. Results and Discussion

3.1 Characterization of Se doped ZnS NPs

The exact concentrations of selenium in the X and Y batches of Se doped ZnS NPs measured from atomic absorption spectrometry analysis were determined to be 2.60 ± 0.12 wt% and 3.50 ± 0.10 wt%, of the as-prepared batches of Se doped ZnS nanoparticles, respectively. The Se concentrations corresponded to mean ± standard deviation of triplicate analysis. The X-ray diffraction patterns of the pristine ZnS NPs and Se-doped ZnS NPs are given in Fig. 1. The characteristic Bragg reflections for the pristine ZnS NPs were located at 28.69^{o}, 47.68^{o}, 56.39^{o},

76.93^{o} and 88.75^{o}, corresponding to (1 1 1), (2 2 0), (3 1 1), (4 0 0) and (3 3 1) planes, respectively of the cubic crystalline structure of ZnS, and matched with JCPDS file number 05-0566. The XRD pattern of Se doped ZnS NPs revealed three important features, *viz.* (a) shift in the XRD peaks to higher 2θ values, i.e., 28.99^{o} (1 1 1), 47.92^{o} (2 2 0) and 56.65^{o} (3 1 1) planes; (b) decreasing order of crystallinity as evident from the decrease in the intensities of the respective diffraction peaks; and (c) broadening of the peaks. The peak shift to higher 2θ value is attributable to doping effect, particularly due to substitution with smaller sized Se^{4+} dopants (0.050 nm) in the lattice sites of ZnS where the ionic radii of Zn^{2+} is 0.060 nm.[34,35] Such a situation would result in the decrease of the lattice parameters of ZnS and consequently lead to lattice distortion. The effect of lattice strain is reflected from the broadening of the XRD peaks for the batch of 2.6 wt % Se doped ZnS NPs, and further broadening was observed for the batch doped with 3.5 wt% Se doped ZnS NPs (Fig. 1). The observed broadening of the XRD peaks could also be due to decrease in the crystallite size.[36] However, the sizes of the as-synthesized ZnS and 2.6 wt% Se doped ZnS NPs were measured by TEM and results are presented in Fig. 2a and 2b, respectively. The particle sizes were observed in the range of 2 and 7 nm with average size of about 3.9 nm (inset of Fig. 2b). Such small particle sizes measured by TEM were corroborated with large BET surface areas, which were measured as 168.4 m^2/g for pristine ZnS NPs and 172.6 m^2/g for 2.6 wt% Se doped ZnS NPs. The crystalline nature of the Se-doped ZnS NPs was confirmed from the high resolution TEM measurement which revealed lattice fringes separated by 0.311 nm, shown in the Fig. 2c and the interatomic spacing was also confirmed in the profile plot (inset of Fig 2c). The inter atomic layer spacings measured in our study was consistent with that reported in literature.[37]

The stabilization of Se doped ZnS NPs of sizes in the range 2 – 7 nm was attributable to effective capping of the nanoparticles by mercaptoactetic acid. Under this scheme, the capping of ZnS NPs by mercaptoacetic acid would necessitate formation of S-S bond. This was confirmed from the FT-IR measurement, where the S-H bond was detected in the mercaptoacetic acid at 2566 cm^{-1} while it was absent in the batches of pristine as well as Se doped ZnS NPs (Fig. 3). In addition, the band observed at 1714 cm^{-1} corresponding to carboxylic acid group in mercaptoacetic acid reagent, was found to shift to 1642 cm^{-1} for Se doped ZnS NPs and 1638 cm^{-1} for pristine ZnS NPs. This shift is implicative of carboxylate group favoring electrostatic interaction between tentative positively charged on ZnS NPs and negatively charged carboxylate ions. It may be argued that such electrostatic interaction rendered stability of the as-synthesized nanoparticles. The colloidal stability of the as-synthesized Se doped ZnS NPs in aqueous medium was also confirmed from the measured value of large zeta potential at neutral pH (ξ = – 44.5 mV). The FT-IR band at 665 cm^{-1} was observed for pristine ZnS NPs and in the Se-doped ZnS NPs, and it was attributed due to Zn-S vibration (corresponding to sulphides).

The band structure of pristine ZnS NPs and Se doped ZnS NPs were determined from the UV-visible absorption spectra (given in Fig. 4). The band gap of the samples was estimated from the absorption edge of Tauc's plot, using the Tauc expression, given below,[38]

$(\alpha hv) = A(hv - E_g)^n$; where α (absorption co-efficient) = (2.303xA)/d

Here *hv, A, d* and E_g are the energy of the incident light, absorbance, path length and band gap, respectively. The value of exponent '*n*' determines the nature of electronic transition. Assuming direct transition (i.e., $n = ½$), the Tauc plot was obtained from $(\alpha hv)^2$ against *hv* and the band gap energy was determined by extrapolating the linear region of $(\alpha hv)^2 = 0$. The band gap of the pristine ZnS NPs, 2.6 wt % and 3.5 wt% Se doped ZnS NPs were determined as 3.84 eV, 3.47

eV and 3.54 eV, respectively. Notably the band gap for pristine ZnS NPs was larger than that of the bulk ZnS (i.e., 3.68 eV), and the increase in the band gap can be attributed to quantum confinement effect in ZnS nanocrystals.[39]

Though the sizes of the Se doped ZnS NPs were similar to those of pristine ZnS NPs, but the batches of Se-doped ZnS NPs revealed narrowing of band gap. This decrease in the band gap for Se doped ZnS NPs can be attributed to structural defects corresponding to interstitial energy levels in the forbidden gap, which could be due to Zn vacancies, sulphur vacancies or cations at interstitial sites, as demonstrated in several cases of doped nanoparticles.[40-42] The structural defects in Se doped ZnS was further evident from the fluorescence emission spectrum, given in Fig. 5a. In addition to a sharp peak at 367 nm, a broad emission peak in the wavelength region of 380 nm – 550 nm was observed. The peak at 367 nm is attributable to near band emission peak. However, the broad peak was associated with a number of small peaks on top of it, which indicated multiple emission peaks in that region. Suitable data deconvulation was performed which revealed emission peaks at 415 nm, 456 nm, 470 nm, 483 nm and 493 nm (Fig. 5b), whose sum peaks fitted well with our experimental data. These emission peaks corresponded to interstates in the Se doped ZnS lattice owing to structural defects. The corresponding energy levels were in the forbidden gap closer to the valence band (shown in Scheme 1). These intermediate energy levels might facilitate interfacial electron (e^-) transfer from the conduction band and hence promote ROS generation and thereby facilitate photocatalytic activity.[43]

3.2. Photocatalytic degradation

The large surface area of Se doped ZnS NPs was favourable for photocatalytic reaction, which is evident from the kinetic studies of sunlight exposed photocatalytic degradation of trypan blue

dye by batches pristine ZnS NPs and Se doped ZnS NPs (Fig 6). Notably, more than 99 % dye degradation was achieved in 3 h for the batch treated with 2.6 wt % Se doped ZnS NPs as compared to only 38 % dye degradation for the batch treated with pristine ZnS NPs. The control experiment for the batch of dye solution treated with Se doped ZnS NPs conducted in the dark condition did not reveal dye removal. This indicated that the adsorption of trypan blue dye on the nanoparticles was negligible. The unfavourable dye adsorption phenomenon can be attributed to negatively charged surface of the nanoparticles at pH 7 (ξ = – 44.5 mV). Similarly, another control experiment was performed to rule out the case of dye degradation due to photolysis, where degradation of dye only due to sunlight exposure was insignificant (Fig. 6). The negative results in both control experiments indicated that dye removal was neither due to its adsorption of dye on nanoparticles nor due to photolysis. It may be concluded that dye removal was due to photocatalytic dye degradation by Se doped ZnS NPs. Further, it was noted that 60% of the dye was degraded in first two hours, and the rate of dye degradation by Se doped ZnS NPs was apparently much faster than other reported metal oxide nanoparticles, e.g., ZnO NPs as photocatalyst.[44] The kinetics of the photocatalytic degradation by pristine ZnS NPs and Se doped ZnS NPs as photocatalyst was studied using Langmuir-Hinshelwood model.[45,46]

$ln(C_o/C) = kt$,

where 'C_o' is the initial concentration of the dye solution, 'C' is the dye concentration at time 't' and 'k' is the pseudo-first order rate constant. From the kinetic studies it was deduced that the photocatalytic dye degradation followed first order kinetics with rate constant k = 0.00316 min^{-1} (R^2 = 0.987) for ZnS NPs and k = 0.02116 min^{-1} (R^2= 0.96) for Se doped ZnS NPs. Notably, the degradation rate constant for Se doped ZnS NPs was seven folds greater than that of ZnS NPs

and was comparable with dye degradation reported for batches of metal oxides assisted with strong oxidizing agents like H_2O_2 as co-catalysts.[19]

In order to evaluate the stability and re-usability of the Se doped ZnS NPs as photocatalyst, three repetitive cycles of degradation process were performed, i.e., equilibration in dark followed by sunlight exposure and recovery of the photocatalyst for subsequent cycle. In all the three cycles, more than 98% degradation of trypan blue dye was achieved in 180 min of sunlight exposure and their respective rate constants (*k*) are given the Fig. 7. Notably, the rate constants of photocatalytic dye degradation determined in each cycle were similar to the test sample (Fig. 6). This indicated that and Se doped ZnS NPs can be efficiently used as a photocatalyst for dye degradation. It may be commented that the drastic improvement in the dye degradation exhibited by Se doped ZnS NPs could be due to high reduction potential of selenium, which is a favorable condition for extraction of photoexcited electrons from conduction band and facilitate generation of ROS.[30]

3.3. Mechanism of dye degradation

3.3.1 Role of Reactive Oxygen Species (ROS)

Light induced generation of free radicals due to the interaction of semiconductor type nanoparticles in aqueous medium is considered to be the key event towards photocatalytic dye degradation.[47,48] In our present study, the role of ROS generation by pristine and Se doped ZnS NPs for photocatalytic dye degradation was confirmed from the terepthalic acid assay, which is selective to hydroxyl radicals.[30] A strong fluorescence emission peak was recorded at λ_{em}= 424 nm which was due to formation of an adduct between ROS and terepthalic acid (Fig. 8). Notably in the absence of sunlight exposure the characteristic peak at λ_{em}= 424 nm was negligible, which

indicated that ROS production was insignificant in the dark condition. It was further noted from the terepthalic acid assay that the intensities of the λ_{em}= 424 nm emission peak was similar for both the batches treated with pristine and Se doped ZnS NPs, though the rate of dye degradation was several fold higher for the batch treated with Se doped ZnS NPs. This indicated that in addition to hydroxyl radicals, Se doped ZnS NPs produced a different type of ROS. It also meant that a different mechanism was involved in the dye degradation by Se doped ZnS NPs when compared to ZnS NPs. It may be commented here that superoxide radicals and singlet oxygen are the other forms of reactive oxygen species that might be generated by metal oxide photocatalyst, and singlet oxygen is eventually one of the end products of superoxide radicals ($O_2^{\cdot -}$).[11,12]

3.3.2 ROS scavenging studies

In order to get an insight of the mechanism of photocatalytic dye degradation by Se doped ZnS NPs, specific ROS scavengers e.g., sodium azide as singlet oxygen scavenger DMSO as hydroxyl radical scavenger and *p*-benzoquinone as superoxide radical scavenger were treated in the reaction medium comprising dye solution and Se doped ZnS NPs as photocatalyst. The kinetic studies of photocatalytic dye degradation in the presence of DMSO and sodium azide are given in Fig. 9a. Compared to the batch treated with sodium azide the rate of inhibition of photocatalytic dye degradation for the batch treated with DMSO was significantly less. This indicated that generation of hydroxyl radicals in the reaction medium was not relevant for Se doped ZnS NPs. On the other hand the photocatalytic dye degradation was significantly inhibited for the batch treated with sodium azide. This is attributable to scavenging of singlet oxygen species from the reaction medium. In other words, it indirectly implied that singlet oxygen

species were generated in the reaction medium by Se doped ZnS NPs. It may be remarked here that the singlet oxygen species are produced due to reaction of holes with superoxide radicals.[11] The tentative generation of superoxide radicals was studied using *p*-benzoquinone as a specific scavenger. Since *p*-benzoquinone is insoluble in water but soluble in ethanol, so the kinetic study of inhibition of dye degradation by *p*-benzoquinone was performed in ethanol-water mixture. Compared to the control batch (i.e. without treating with *p*-benzoquinone), 1 mM solution of freshly re-crystallized ethanolic solution *p*-benzoquinone was capable of inhibiting trypan blue dye degradation (Fig. 9b). This indirectly implied that superoxide radicals ($O_2^{\cdot -}$) were generated in the reaction medium during the interaction with Se doped ZnS NPs. In this study it was however not possible to compare the extent of generation of superoxide radicals and singlet oxygen species from the rate of inhibition of dye degradation by *p*-benzoquinone (superoxide radical scavengers) and that by sodium azide (singlet oxygen scavenger), respectively as these studies were performed in different solvent system. However, singlet oxygen species are formed from the superoxide radicals and hence it may be remarked that both superoxide radicals and singlet oxygen species were generated in the reaction medium and were responsible for dye degradation.

As the ROS generation is based on scavenging action so it was necessary to confirm that sodium azide does not scavenge hydroxyl radicals. The hydroxyl radicals were generated in batches of dye solution (without treating with photocatalyst) by spiking suitable concentrations of H_2O_2 and exposed to UV light (λ =360 nm). These batches were treated respectively with sodium azide and DMSO. As expected, the batch of dye solution treated with sodium azide did not inhibit dye degradation while the batch treated with DMSO revealed inhibition of dye degradation (Fig. 10a). This clearly explained that sodium azide cannot scavenge hydroxyl radicals. The role of

sodium azide in scavenging singlet oxygen species was also revealed from the increase in the rate of inhibition of dye solution by increasing sodium azide concentration, where the batch treated with 200 mM sodium azide completely inhibited dye degradation (Fig. 10b). It may therefore be concluded that the drastic inhibition of dye degradation observed in the test samples (shown in Fig. 9a) by sodium azide was due to scavenging of singlet oxygen species which were generated in the reaction medium due to interaction of se doped ZnS NPs with dye solution.

3.3.3. Band structure of Se doped ZnS NPs and singlet oxygen generation

Now in order to account for the role of singlet oxygen towards photocatalytic dye degradation by Se doped ZnS NPs, it is important to understand the electronic band structure and possible charge transport phenomenon in Se doped ZnS NPs. The electronic structure of Se doped ZnS NPs given in scheme 1 with an assumption that the structure was similar to ZnS NPs without Se doping. The electronic structure was characterized by the band gap energy (E_g) corresponding to the differences between the valence band (E_{VB}) and the conduction band (E_{CB}), each comprising of a high density of states. The conduction band edge minima (E_{CB}) and valence band maxima (E_{VB}) of the semiconductor like materials of Se doped ZnS NPs as photocatalysts could be empirically calculated using the following expressions with Nerstian correction for pH: [49,50]

$E_{CB} = \chi(A_aB_b) - ½E_g + E_{o;}$ and the pH corrected expression $E_{CB,(pH)} = E_{CB} + 0.059\ (PZZP\text{-}pH)$ and

$E_{VB} = E_{CB} + E_g$; and the pH corrected expression, $E_{vb(pH)} = E_{VB} + 0.059\ (PZZP\text{-}pH)$

where, E_g is the band gap of Se-ZnS NPs, E_{CB} is the potential of the conduction band, E_{VB} is the potential of valence band, E_o is the scale factor taken as – 4.50 eV, i.e., the energy of free

electrons on the normal hydrogen electrode (NHE scale). The parameter $\chi(A_aB_b)$ corresponds to the absolute electronegativity of a semiconductor material type A_aB_b, which is calculated as the geometric mean of the electronegativity of the constituent atoms[51]. In our calculation, the electronegativity values for Zn and S were taken as 4.45 eV, and 6.22 eV, respectively. From the above expressions, the energy levels of conduction band and the valence band were calculated as −1.17 eV and +2.29 eV, respectively. These energy levels are important parameters that decide the feasibility of charge transport of photoexcited electrons and holes to the surface of the nanoparticles and subsequent interacting with the molecular oxygen and water, respectively to produce the reactive oxygen species. The redox potentials for $O_2/O_2^{\cdot-}$ and $H_2O/OH^{\cdot}$ is given as −0.2 eV and +2.2 eV, respectively in the NHE scale (shown in scheme 1).[52] Apparently in the case of Se doped ZnS NPs, the charge transport is favourable for both photoexcited electrons from conduction band to the redox couple of molecular oxygen to form superoxide radicals and holes from valence band to the redox couple of H_2O to form hydroxyl radicals. But our ROS scavenging studies revealed that only superoxide radicals and singlet oxygen were generated while generation of hydroxyl radical was not convincing. It may be remarked here that the holes generated in our system were utilized for converting superoxide radicals to singlet oxygen as given in Scheme 1.[11]

Moreover the dye degradation efficiency of Se doped ZnS NPs was several folds higher than pristine ZnS NPs. The major difference between pristine ZnS NPs and Se doped ZnS NPs corresponded to the structural defects in the doped NPs. The fluorescence emission spectrum of Se doped ZnS clearly revealed the existence of energy levels in the forbidden gap of the nanocrystals of Se doped ZnS owing to structural defects. Therefore the photoexcited electrons

in the conduction band could either hop to the surface of the nanocrystals, trapped in the defect sites or re-combine with holes. Under such circumstances, the reduction of molecular oxygen at the surface of the nanoparticles by photoexcited electron is more likely, which would facilitate enhanced photocatalytic dye degradation mediated by superoxide radicals and singlet oxygen. Further studies would be required to understand in more details about the importance of structure – activity relationship in semiconductor nanoparticles.

4. Conclusion

The doping of ZnS NPs with selenium resulted in narrowing of the band gap corresponding to visible region. The two salient features of this study were (a) achievement of more than 99 % sunlight induced photocatalytic dye degradation in 3 h by 2.6 wt% Se doped ZnS as compared to 38 % dye degradation by pristine ZnS NPs; (b) seven fold increase in the rate of dye degradation by Se doped ZnS over pristine ZnS. Such a drastic improvement in the photocatalytic behaviour was attributed to consequences of doping with selenium leading to structural defects, e.g., formation interstitial energy levels in the doped ZnS lattice. As a result the photoexcited electron-hole transport was altered and favoured, which impacted on the generation of the nature of reactive oxygen species (ROS). Specific ROS scavenger assay by sodium azide and *p*-benzoquinone confirmed that superoxide radicals and singlet oxygen, which were primarily generated in the reaction medium by Se-doped ZnS NPs, triggered the degradation of trypan blue. The experimental results were well supported by theoretical band structure calculation which favoured transportation of electrons from conduction band to interact with oxygen molecules to produce superoxide radicals and singlet oxygen species.

Acknowledgement

One of the authors (S.T.) is thankful to Ministry of Human Resource Development (MHRD), Govt of India for awarding Senior Research Fellowship. Authors are thankful for the instrumental facilities of the Institute Instrumentation Centre, Department of Chemistry and Centre of Nanotechnology, IIT Roorkee.

References

1. L. Pereira and M. Alves, *Environmental Protection Strategies for Sustainable Development*, Ed. A. Malik and E. Grohmann, Springer, New York, 2012, Vol. **14**, pp.111–162.
2. M. Perez, F. Torrades, X. Domenech and J. Peral, *Water Res.*, 2002, **36**, 2703-2710.
3. S. S. Boxi and S. Paria, *RSC Adv*. 2015, **5**, 37657-37668
4. P. V. R. K. Ramacharyulu, D. B. Nimbalkar, J. P. Kumar, G. K. Prasad and S.-C, Ke, *RSC Adv.,* 2015, 5, 37096-37101
5. M. M. Khin, A. S. Nair, V. J. Babu, R. Murugana and S. Ramakrishna, *Energy Environ. Sci.*, 2012, **5**, 8075–8109.
6. X. Hu, G. Li, and J. C. Yu, *Langmuir*, 2010, **26** (5), 3031–3039.
7. R. K. Dutta, B. P. Nenavathu, M. K. Gangishetty and A. V. R. Reddy, *J. Environ. Sci. Heal. A*, 2013, **48**, 871-878
8. S. Guo, G. Zhang and J. Wang, *J. Colloid Interface Sci*., 2014, **433**, 1–8.
9. G. Pliego, J. A. Zazo, J A. Casas and J. J. Rodriguez, *J. Hazard. Mater.*, 2013, **252– 253**, 180– 185.

10. J. Paul, K. P. Rawat, K. S. S. Sarma and S. Sabhrawal, *Appl. Radiat. Isotopes,* 2011, **69**, 982–987.

11. T. Tachikawa and T. Majima, *Langmuir,* 2009, **25**(14), 7791–7802.

12. R. K. Dutta, B. P. Nenavathu, M. K. Gangishetty and A. V. R. Reddy, *Colloids Surf. B,* 2012, **94**, 143–150.

13. H. Jia, W. He, W. G. Wamer, X. Han, B. Zhang, S. Zhang, Z. Zheng, Y. Xiang and J. –J. Yin, *J. Phys. Chem. C,* 2014, **118**, 21447−21456.

14. T. Tachikawa, M. Fujitsuka, T. Majima, *J. Phys. Chem. C*, 2007, **111**, 5259–5275.

15. A. Lipovsky, Z. Tzitrinovich, H. Friedmann, G. Applerot, A. Gedanken and R. Lubart, *J. Phys. Chem. C*, 2009, **113**(36), 15997–16001.

16. Y. Murakami, E. Kenji, A. Y. Nosaka and Y. J. Nosaka, *Phys. Chem. B*, 2006, **110**, 16808–16811.

17. S. G. Kumar and K. S. R. K. Rao, *RSC Adv*., 2015, **5**, 3306–3351

18. S. H. Shen T. Chan, W. Yeong, J. C. Juan and C. Y. Teh, *J. Chem. Technol. Biotechnol.,* 2011, **86**, 1130–1158.

19. A. Sharma and R. K. Dutta, *RSC Adv*., 2015, **5**, 43815–43823.

20. M. R. Hoffmann, S. T. Martin, W. Choi and D. W. Bahnemann, *Chem. Rev.*, 1995, **95,** 69–96.

21. D. Das and R. K. Dutta, *J. Colloid Interface Sci.* 2015, **457**, 339–344.

22. Z. Xiong, L. L. Zhang, J. Ma, X. S. Zhao, *Chem. Commun.* 2010, **46**, 6099-6101.

23. M. Sharma, T. Jain, S. Singh and O. P. Pandey, *Solar Energy,* 2012, **86**, 626–633.

24. R. K. Dutta, U. C. Bind, J.B.M. Krishna, A.K. Sinha and G. S. Taki, *J. Radioanal. Nucl. Chem.* 2014, **302,** 819-824

25. S. Joicy, R. Saravanan, D. Prabhu, N. Ponpandian and P. Thangadurai *RSC Adv.,* 2014, **4,** 44592-44599.

26. A. Kudo and M. Sekizawa, *Chem. Commun*., 2000, 1371-1372.

27. K. Wang, Y. Shi, H. Zhang, Y. Xing, Q. Dong, and T. Ma, *Phys. Chem. Chem. Phys*., 2014, **16**, 23316-23319

28. N. T. Hahn, A. J. E. Rettie, S. K. Beal, R. R. Fullon, and C. B. Mullins, *J. Phys. Chem. C*, 2012, **116**, 24878−24886

29. J. Qian, K. Jiang, J. Huang, Q. Liu, L.Yang and Y. Song, *Angew. Chem*., 2012, **124**, 10497–10500.

30. B. P. Nenavathu, A. V. R. K. Rao, A. Goyal, A. Kapoor and R. K. Dutta, *Appl. Catal. A.,* 2013, **459**, 106–113.

31. E. D. Kerver, I. M. C. Vogels, K. S. Bosch, H. V. S. Rova, R. J. M. Vandenmunckhof and W. Frederiks, Histochem. J., 1997, **29**, 229–237.

32. J. R. Harbour and S. L. Issler, *J. Am. Chem. Soc.*, 1982, **104** (3), 903–905.

33. M. Sahni and B. R. Locke, *Ind. Eng. Chem. Res.*, 2006, **45**, 5819-5825.

34. R. Dong, Q. Ye, L. Kuang, X. Lu, Y. Zhang, X. Zhang, G. Tan, Y. Wen and F. Wang, *ACS Appl. Mater. Interfaces,* 2013, **5**, 9508−9516.

35. M. Kurian and C. Kunjachan, *Int. Nano Lett*., 2014, **4**, 73–80.

36. R. J. Wiglusz, A. Bednarkiewicz, and W. Strek, *Inorg. Chem.,* 2012, **51**, 1180−1186.

37. Y. P. Zhu, J. Li, T. Y. Ma, Y. P. Liu, G. Du, and Z. Y. Yuan. *J. Mater. Chem. A*, 2014, **2**, 1093–1101.

38. A. Beleanu, M. Mondeshki, Q. Juan, F. Casper, C. Felser and F. Porcher, *J. Phys. D: Appl. Phys.,* 2011, **44**, 475302.

39. A. P. Alivisatos, *Science*, 1996, **271 (5251)**, 933-937

40. Z. Fang, S. Weng, X. Ye, W. Feng, Z. Zheng, M. Lu, S. Lin, X. Fu, and P. Liu, *Appl. Mater. Interfaces,* 2015, **7**, 13915−13924.

41. D. Mocatta, G. Cohen, J. Schattner, O. Millo, E. Rabani, and U. Banin, *Science*, 2011, **332**, 77-81

42. W. Zhu, X. Qiu, V. Iancu, X. Q. Chen, H. Pan, W. Wang, N. M. Dimitrijevic, T. Rajh, H. M. Meyer III, M. P. Paranthaman, G. M. Stocks, H. H. Weitering, B. Gu, G. Eres and Z. Zhang, *PRL, 2009,* **103**, 226401-226404

43. R. K. Dutta, B. P. Nenavathu and M. K. Gangishetty*, J. Photochem. Photobiol., B*, 2013, **126**, 105–111.

44. R. K. Dutta, B. P. Nenavathu and S. Talukdar, *Colloids Surf. B*, 2014, **114,** 218– 224

45. Y. S. Ho, J. C. Y. Ng and G. McKay, *Separ. Purif. Method.*, 2000, **29** (2), 189–232.

46. J. Li, F. Sun, K. Gu, T. Wu, W. Zhai, W. Li and S. Huang, *Appl. Catal., A*, 2011, **406**, 51–58.

47. D. Channei, B. Inceesungvorn, N. Wetchakun, S. Ukritnukun, A. Nattestad, J. Chen and S. Phanichphant, *Nature*, 2014, **4**, 5757

48. D. Beydoun, R. Amal, G. Low and S. McEvoy, *J. Nanopart. Res.,* 1999, **1**, 439–458.

49. R. R. Reddy, Y. N. Ahammed, K. R. Gopal and D. V. Raghuram, *Opt. Mater*., 1998, **10**, 95–100.

50. Y. Xu and M. A. A. Schoonen, *Am. Mineral*., 2000, **85**, 543–556.

51. R. G. Pearson, *Inorg. Chem*. 1988, **27**, 734-740.

52. Y. Li, W. Zhang, J. Niu, and Y. Chen, *ACS Nano*, 2012, **6**, 5164–5173.

FIGURE CAPTION

Fig. 1. X-Ray diffraction (XRD) pattern of Pristine ZnS NPs, 2.6 wt% Se-doped ZnS NPs and 3.5 wt% Se-doped ZnS NPs

Fig. 2. Transmission electron microscopy (TEM) images of (a) pristine ZnS NPs; (b) 2.6 wt% Se-doped ZnS NPs; (inset: size distribution histogram of 2.6 wt% Se-doped ZnS NPs); (c) High resolution TEM (HRTEM) image of 2.6 wt% Se doped ZnS NPs showing lattice fringes marked by the arrows; (inset: profile image of the lattice fringes)

Fig. 3. Fourier transformed infrared (FT-IR) spectra of (a) mercaptoacetic acid (MAA) used as capping agent; (b) 2.6 wt% Se doped ZnS NPs capped with MAA; and (c) pristine ZnS NPs capped with MAA

Fig. 4. Showing Tauc's plot obtained from UV-visible absorption spectroscopy of pristine ZnS NPs and 2.6 wt% Se-doped ZnS NPs and 3.5 wt% Se doped ZnS NPs

Fig. 5. Fluorescence emission spectra of (a) pristine ZnS NPs and (b) 2.6 wt% Se-doped ZnS NPs

Fig.6. Sunlight induced kinetic studies of degradation of trypan blue dye treated with batches of pristine ZnS NPs; 2.6 wt% Se-doped ZnS NPs and control batch of dye solution without treating with any nanoparticles

Fig.7. Sunlight induced kinetic study showing re-usability of the photocatalyst for sustained efficiency in dye degradation performed for three successive cycles

Fig.8. Terepthalic assay profile for hydroxyl radical generation in presence of photocatalysts (pristine ZnS and 2.6 wt % Se doped ZnS NPs), both in dark condition and under sunlight exposure

Fig. 9. Showing kinetic studies of inhibition of trypan blue dye degradation treated with 2.6 wt% Se doped ZnS NPs as photocatalyst exposed to sunlight for batches (a) in presence of sodium azide as singlet oxygen scavenger and DMSO as hydroxyl radical scavengers; (b) in presence of *p*-benzoquinone (BQ) as superoxide radical scavenger

Fig. 10. (a) Showing the consequences of mimicking hydroxyl radical generation towards dye degradation in the batches of trypan dye solution treated with DMSO (hydroxyl radical scavenger) and sodium azide (singlet oxygen scavenger); (b) showing effect of varying concentration of sodium azide on the rates of inhibition of dye degradation

Scheme 1: Schematic diagram showing energy levels of valence band, conduction band and interstates of the 2.6 wt% Se doped ZnS NPs in NHE scale and its suitability of photocatalytic degradation of trypan blue dye

FIGURES

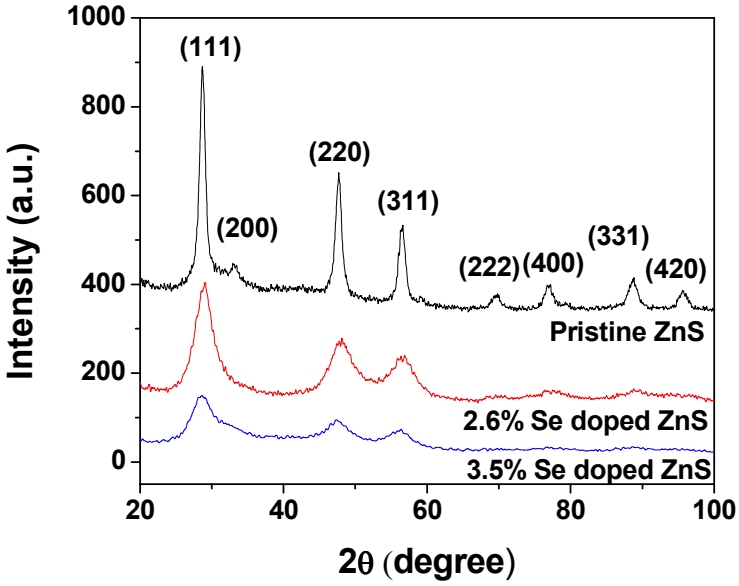

Fig. 1

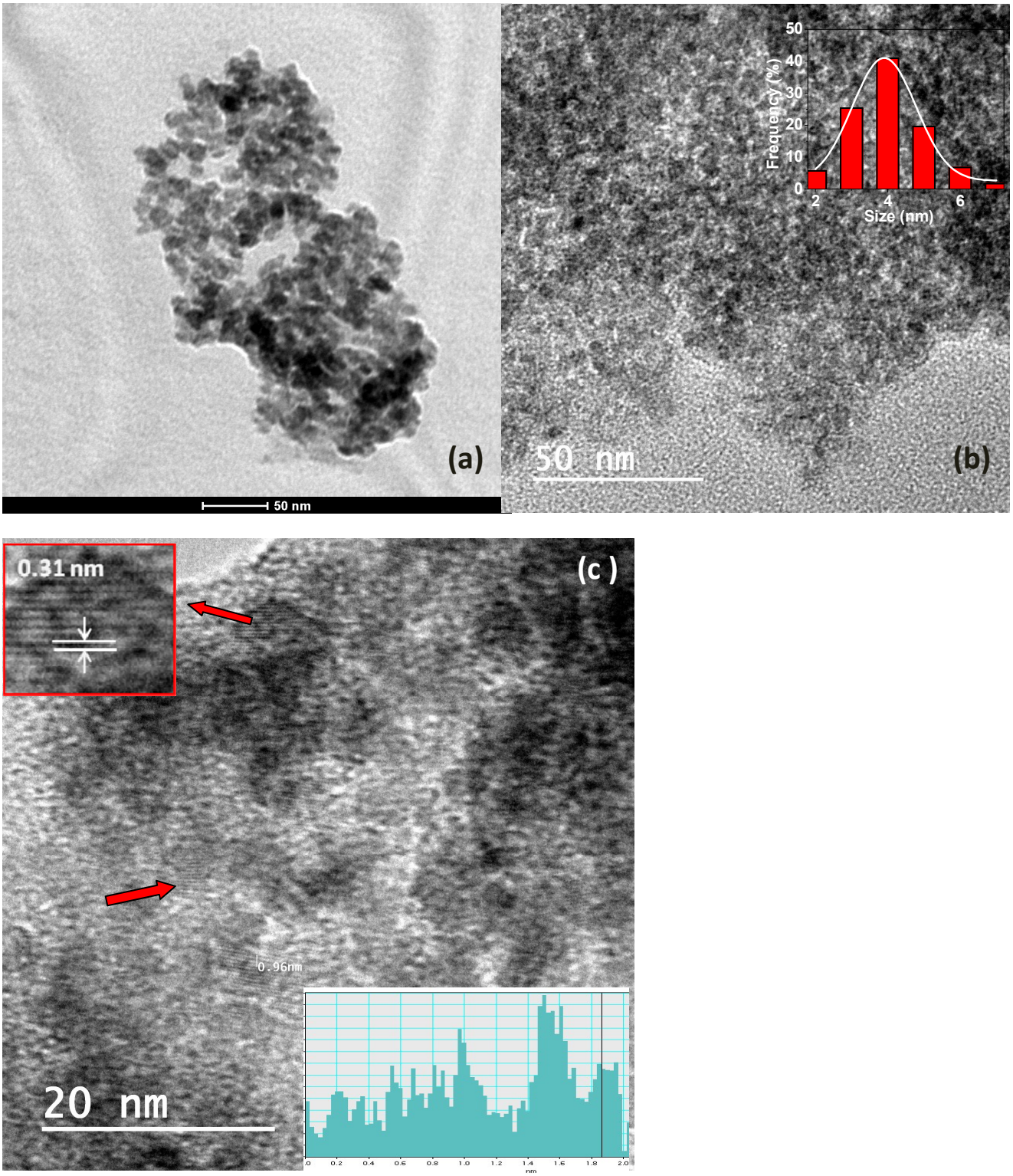

Fig. 2.

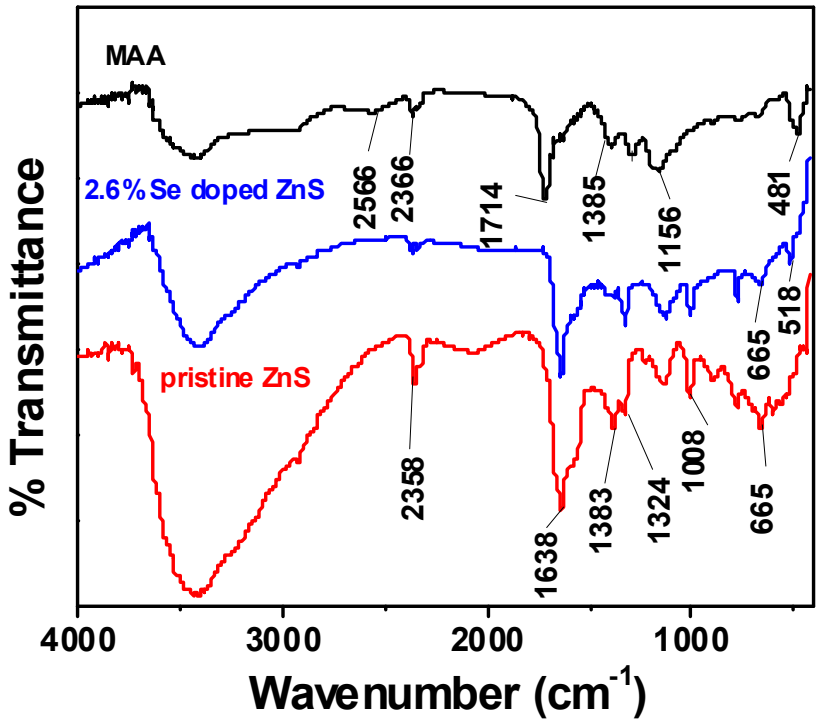

Fig. 3.

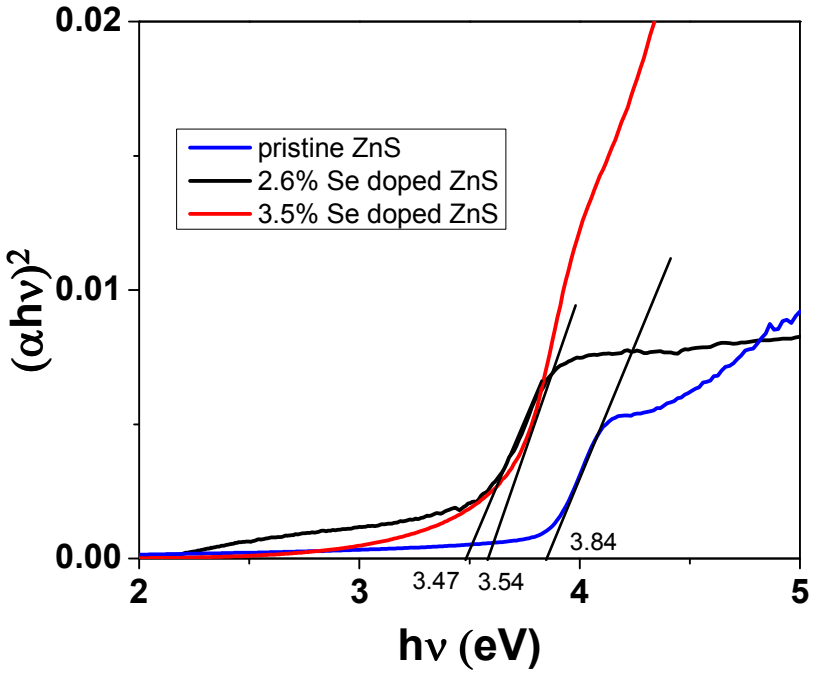

Fig. 4.

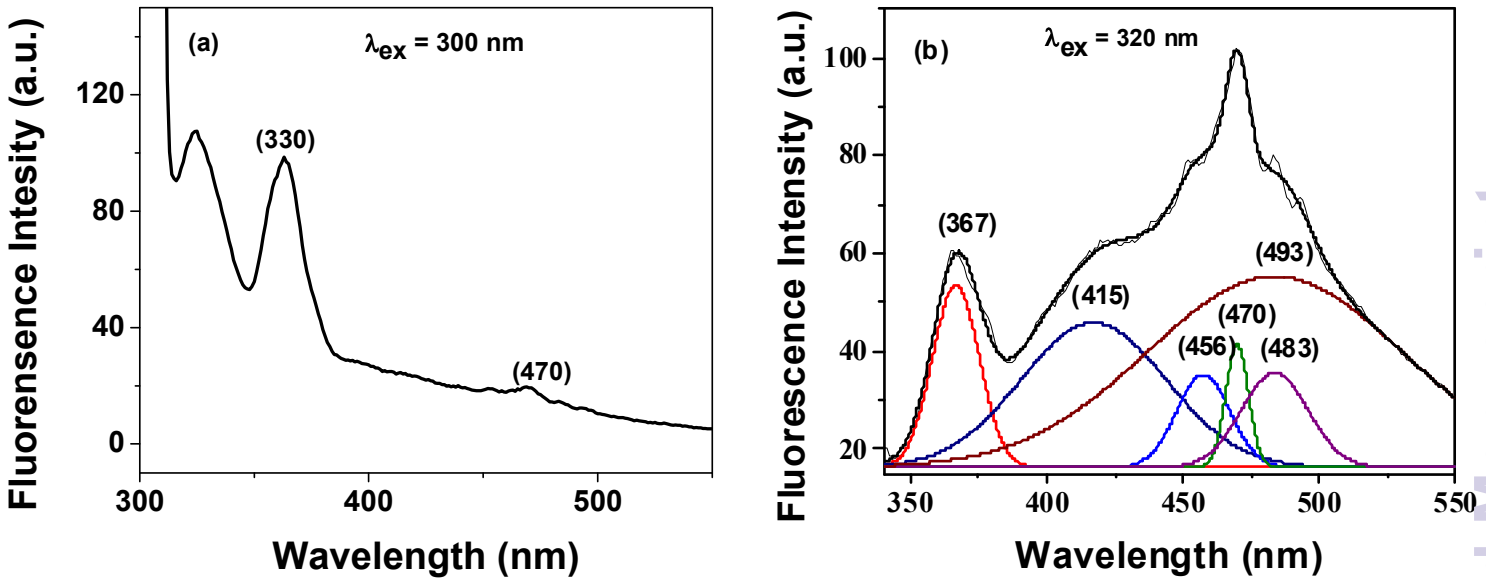

Fig. 5.

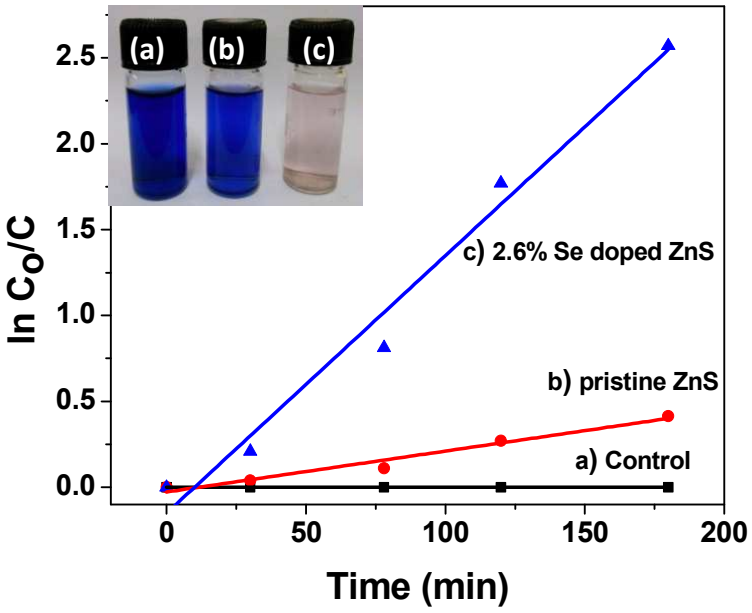

Fig. 6.

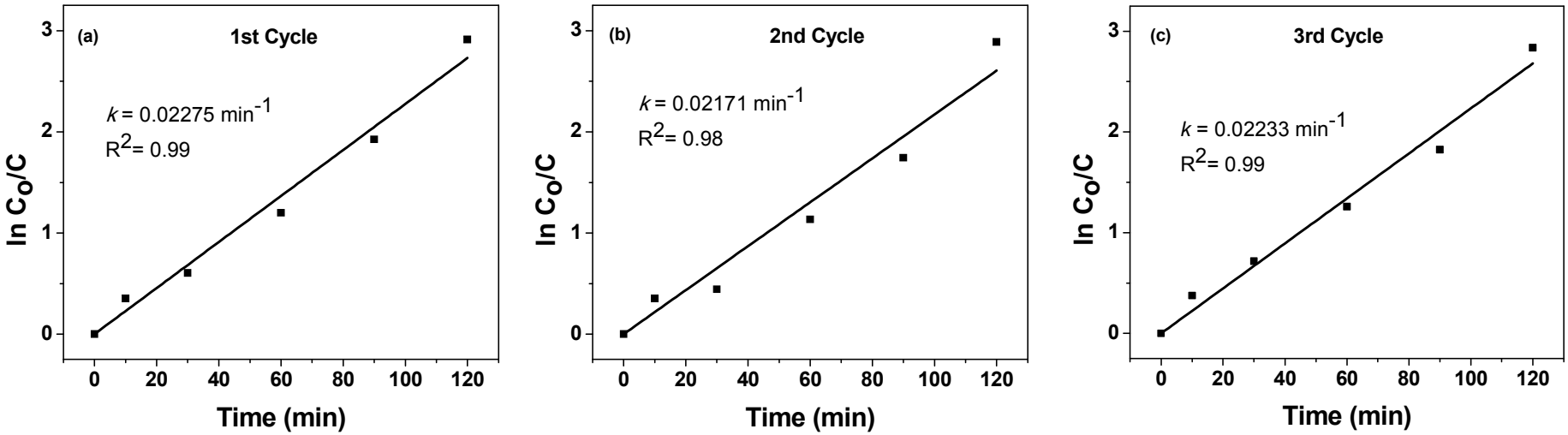

Fig. 7.

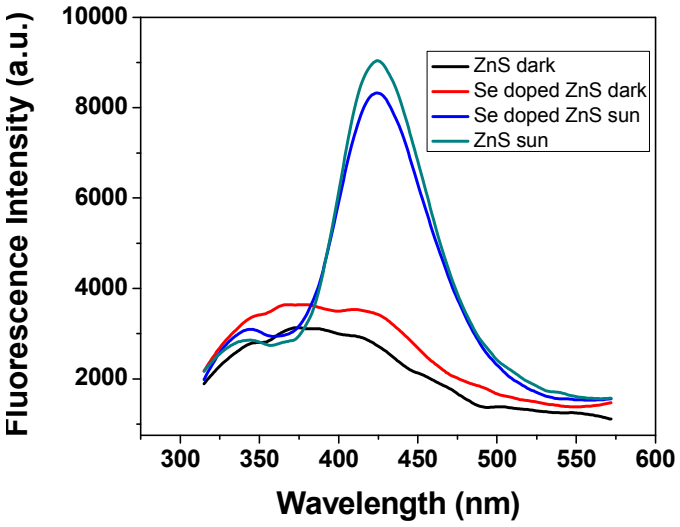

Fig. 8.

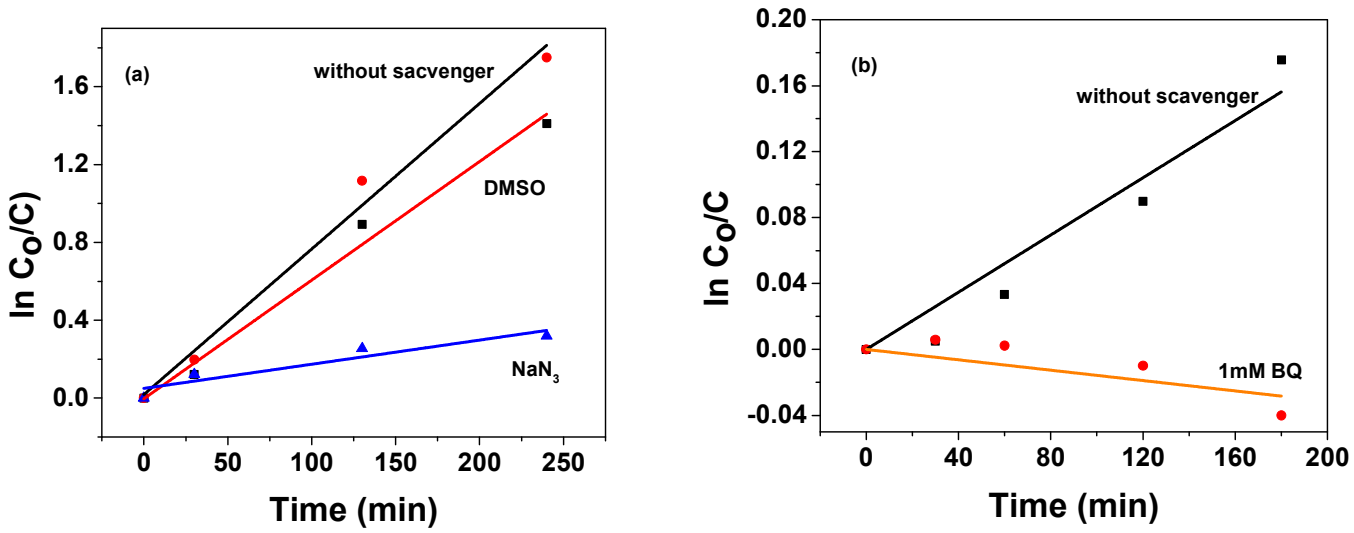

Fig. 9.

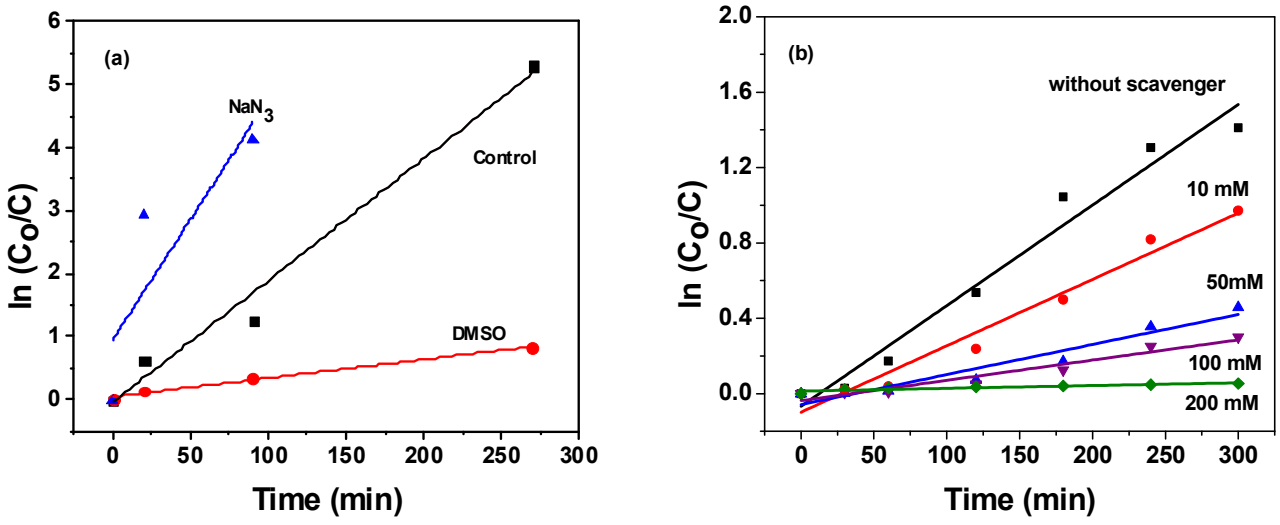

Fig. 10

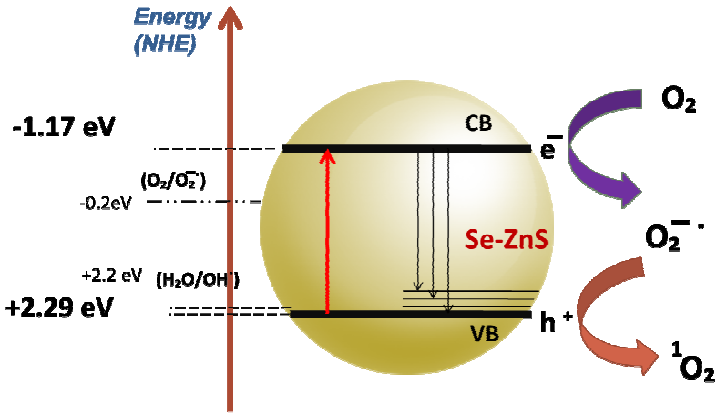

Scheme 1.

A mechanistic approach for superoxide radicals and singlet oxygen mediated enhanced photocatalytic dye degradation by selenium doped ZnS nanoparticles

Soumita Talukdar, Raj Kumar Dutta*

Department of Chemistry, Indian Institute of Technology Roorkee, Roorkee 247667, India

* Corresponding Author, Email address: duttafcy@iitr.ac.in (R.K. Dutta), Tel: +91 1332 285280, Fax: +91 1332 286202

Graphical Abstract

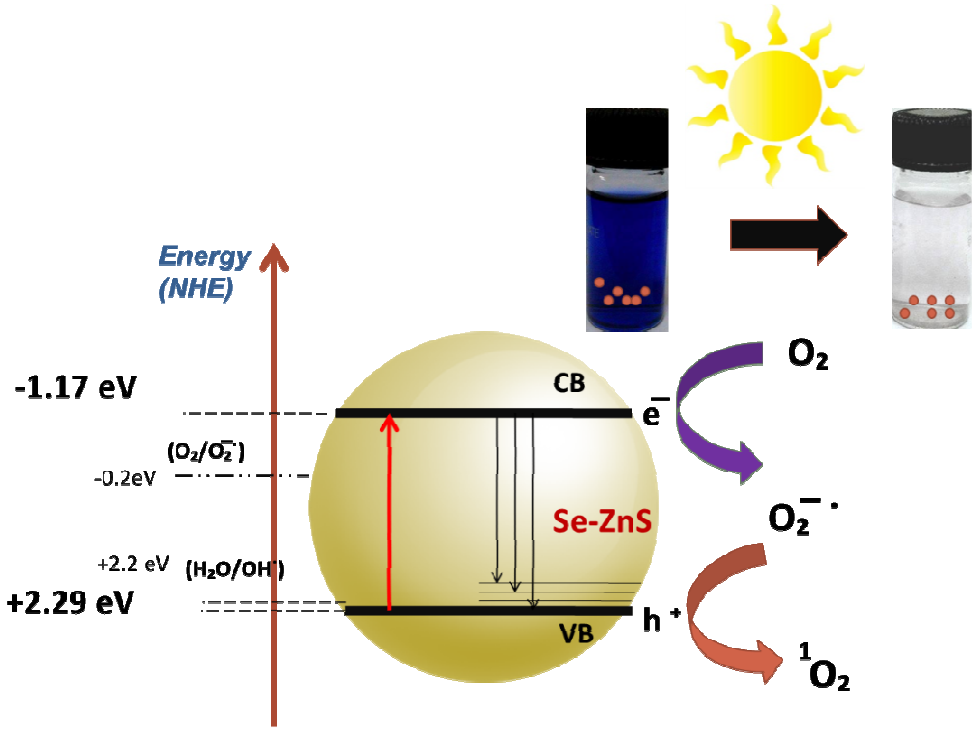

Superoxide and singlet oxygen mediated photocatalytic dye degradation by Se doped ZnS NPs